Research Square

Preprints are preliminary reports that have not undergone peer review.
They should not be considered conclusive, used to inform clinical practice,
or referenced by the media as validated information.

Comparative Evaluation of RL-TD3 PID Control against Hybrid and Conventional Optimizers in Renewable -Based Islanded Microgrids

Dana Rajaa Shaaban
Electrical Engineering Technical College, Middle Technical University
Ali Nasser Hussain
Electrical Engineering Technical College, Middle Technical University
Ahmed K. Ali
engineer28ahmed@gmail.com
Polytechnic College of Engineering–Baghdad, Middle Technical University
Mohammed Alruwaili
Northern Border University
Moustafa Ahmed Ibrahim
University of Business and Technology

Article

Keywords: Reinforcement Learning, Twin Delayed Deep Deterministic Policy Gradient (TD3), Islanded Microgrids, PID, Renewable Energy, Load Frequency Control

Posted Date: July 10th, 2026

DOI: https://doi.org/10.21203/rs.3.rs-10232537/v1

License: This work is licensed under a Creative Commons Attribution 4.0 International License.
Read Full License

Additional Declarations: No competing interests reported.

Comparative Evaluation of RL-TD3 PID Control against Hybrid and Conventional Optimizers in Renewable -Based Islanded Microgrids

Dana Rajaa Shaaban[1], Ali Nasser Hussain[1], Ahmed K. Ali[2, *], Mohammed Alruwaili[3], Moustafa Ahmed Ibrahim[4, *]

[1]Department of Electrical Power Engineering Techniques, Electrical Engineering Technical College, Middle Technical University, Baghdad 10074, Iraq.

[2]Polytechnic College of Engineering–Baghdad, Middle Technical University, Baghdad 10074, Iraq.

[3]Department of Electrical Engineering, College of Engineering, Northern Border University, Arar 91431, Saudi Arabia.

[4]Electrical Engineering Department, University of Business and Technology, Jeddah 23435, Saudi Arabia.

Dana Rajaa Shaaban; Email**:** BCC5001@mtu.edu.iq

Ali Nasser Hussain; Email**:** dr_alinasser@mtu.edu.iq

Ahmed K. Ali; Email: engineer28ahmed@gmail.com

Mohammed Alruwaili; Email**:** mohamedalrowelli@gmail.com

Moustafa Ahmed Ibrahim; Email**:** m.ibrahim39@outlook.com

***** Corresponding Authors.

Comparative Evaluation of RL-TD3 PID Control against Hybrid and Conventional Optimizers in Renewable -Based Islanded Microgrids

Abstract:

The growing contribution of renewable energy sources to island microgrids presents major obstacles to load frequency control (LFC), mainly because of low system inertia, unreliable generation, and unpredictable load dynamics. These contribute greatly to the deterioration of frequency stability and the design of controllers. The paper is a comparative analysis of a reinforcement learning (RL)-based Twin Delayed Deep Deterministic Policy Gradient (RL-TD3)-optimized proportional-integral-derivative (PID) controller along with optimization-based tuning methods. The proposed RL-TD3 model allows the problem-specific online, data-driven fine-tuning of PID gains, thus improving the adaptability and resilience to various operating conditions and disturbances. To evaluate the effectiveness of control, the RL-TD3 PID controller is compared with a Coati Optimization Algorithm (COA) and hybrid optimization algorithms such as the Grey Wolf Optimization Algorithm with Cuckoo Search (GWO-CS). All tuning methods are assessed based on standard dynamic performance measures of settling time, overshoot, steady-state error, and integrals of time-weighted measures, such as the Integral of Time-weighted Absolute Error (ITAE) and the Integral of Time-weighted Squared Error (ITSE). The results of the simulation show that the RL-TD3-based PID controller is always better in terms of faster dynamic response, better disturbance rejection, and greater resistance to the system uncertainties and changes in parameters. The results also show the effectiveness of deep RL agent combined with PID structures in microgrid systems for LFC applications. The study provides important insights to compare merits of various optimization algorithms and make the RL-TD3 a promising approach to reliable and efficient frequency regulation in renewable-based islanded microgrids.

Keywords: Reinforcement Learning, Twin Delayed Deep Deterministic Policy Gradient (TD3), Islanded Microgrids, PID, Renewable Energy, Load Frequency Control.

1 INTRODUCTION

The use of RES in island microgrids creates problems for maintaining frequency stability because of two factors which include reduced system inertia and unpredictable power generation and load changes. LFC systems become less effective when they face nonstandard

operating conditions which cause system parameters to change and create unpredictable patterns of disturbances [1]. The control systems have an urgent requirement to develop new control methods which will ensure that microgrids with RES will maintain their frequency stability at all times.

The control system design field has found RL to be an effective control system design method because it uses data for control system design to create adaptable systems that can learn optimal policies from dynamic environments[2]. As reported in recent work printed in[3], authors proposed an adaptive PID-based load frequency control (LFC) strategy for an islanded microgrid system comprising heterogeneous distributed energy resources and an energy storage system (ESS). The study addressed the limitations of conventional PID controllers, whose fixed gains are unable to maintain satisfactory frequency regulation under varying operating conditions and renewable energy uncertainties. In order to overcome these challenges, two deep reinforcement learning algorithms, Deep Deterministic Policy Gradient (DDPG) and Twin Delayed Deep Deterministic Policy Gradient (TD3), are employed to adaptively tune the PID controller gains in real time. The RL agents were trained offline using a reward function designed to minimize frequency deviations and subsequently implemented online for continuous gain adjustment using the PID controller. Comparative simulation results demonstrated that both DDPG-based and TD3-based adaptive PID controllers significantly outperformed the conventional PID controller in terms of robustness against load disturbances. Moreover, the TD3-based controller achieved superior performance compared with the DDPG-based controller by providing faster convergence, enhanced stability, and reduced oscillatory behaviour owing to its improved policy update mechanism and mitigation of value overestimation.

The TD3 algorithm achieves better stability and convergence performance than previous actor–critic methods, which include all RL techniques. The RL-TD3 system improves system performance by enabling real-time control gain tuning through its combination with traditional PID controllers [4]. The evaluation of RL-TD3-based PID control effectiveness requires testing its performance against standard optimization methods and hybrid/metaheuristic optimization techniques.

Conventional tuning methods for PID controllers, such as Ziegler–Nichols and trial-and-error procedures, establish baseline performance standards [5]. In literature, several metaheuristic optimization algorithms have been proposed for tuning the PID controller in microgrids [6 78910].

A recent heuristic optimization algorithm used for improving the operational performance of microgrids as techno-economics with renewable sources has been discussed from their primary

historically developed source [6]. The operational performance of microgrids includes energy management optimization, cost-effective dispatch, dependability, storage sizing, cyberattack minimization, and grid integration. In [7], a study was conducted on LFC in a microgrid that utilizes renewable energy sources, employing a PID controller optimized by comparing the performances of four evolutionary optimization algorithms. The performance compared the optimized PID controller under various operating scenarios.

In [8], a crayfish optimization algorithm (COA) is compared to conventional algorithms like the genetic algorithm (GA) and spotted hyena optimizer (SHO) for integrated photovoltaic AC/DC microgrid converters. The COA optimizer is designed to adjust the controller gains automatically as the system changes so as to improve the performance of voltage boosting of microgrid converters. In [9], a study was conducted on LFC and tie-line power flow in multi-interconnected microgrids that use renewable energy sources and experience continuous load changes, employing a hybridized algorithm that combines the exploration capabilities of particle swarm optimization (PSO) with the exploitation capabilities of grey wolf optimization (GWO). This integrated optimization scheme aims to optimize the gains of the PID sensor and cascade proportional integral–proportional derivative (PI–PD) controller to obtain higher control accuracy and dynamic stability. In the same context [10], employing a GWO algorithm for optimized PID controller parameters of the two-area multi-microgrid (MMG) system with a tie-line that utilizes renewable energy sources,

Hybrid metaheuristic optimization algorithms combine two search algorithms to improve the exploration search of the new combined algorithm. A hybrid optimizer delivers better global search performance and has been used to tune PID controllers for LFC microgrids, such as GWO-CS [11]. The hybrid optimization algorithm required extensive computational resources, and it was complex to select a balance of hyperparameters. In addition, the metaheuristic optimization algorithms are also used for tuning PID control, such as COA [4], and PSO [12].

It appears that most of the literature focuses on using the optimization algorithm in tuning PID control in the LFC of microgrids, which have some drawbacks in the case of random load disturbance. Therefore, this paper conducts a complete assessment of RL-TD3-based PID control compared to traditional optimization methods and hybrid optimization methods within the context of renewable energy IMGs. The assessment process evaluates system performance through two main criteria that test system robustness and adaptive capabilities and their ability to return to a normal state after different types of disturbances and system uncertainty challenges. Furthermore, the assessment of each individual approach requires a structured

comparison method to calculate performance improvements, which must measure basic dynamic indexes such as settling time, overshoot, and steady-state error, as well as integral performance criteria including ITAE and ITSE [3].The contributions of this paper can be summarized as follows:

1. A TD3-based RL agent framework has been developed to adaptively control a PID controller in an IMGs for the LFC against variability in renewable generation and load disturbances.
2. A dynamic simulation model of IMG has been developed to demonstrate the dynamic performance effectiveness of the proposed RL-TD3-PID controller for frequency regulation in IMGs.
3. The proposed RL-TD3-PID controller enables online, data-driven adaptation, improving robustness against renewable generation variability, load disturbances, and low-inertia system conditions.
4. A comprehensive comparative study is conducted between the proposed method and metaheuristic approaches, including the COA and GWO-CS.

The paper is structured as follows: section 2 presents the mathematical model of the IMG, section 3 represents the TD3 algorithm, section 4 represents the optimization techniques, section 5 provides the simulation results, and section 6 presents the conclusion.

2 MATHEMATICAL MODEL OF THE ISLANDED MICROGRID

The dynamic behavior of an islanded microgrid system with its distributed energy resources and load systems and energy storage components operates in autonomous mode according to its mathematical model. The IMG needs to control its frequency and voltage through internal methods because grid connection is not available, which requires precise dynamic simulations of all its system elements. The system functions through a collection of nonlinear differential equations which scientists develop from power balance equations and generator swing equations and converter control system equations [13]. The frequency dynamics become accessible through analysis of power generation differences while the inverter-interfaced DERs use droop control characteristics to mimic synchronous generator performance. Distributed controllable generators such as diesel engine generator (DEG), fuel cells (FC) and biogas turbine generator (BGTG) are represented in first order transfer functions. Energy storage devices (ESS) such as batteries (BES), flywheels (FESS) and electric vehicles (EV) are often

represented through first-order transfer functions which enable them to demonstrate their ability to quickly respond to transient disturbances. In addition to renewable sources like solar photovoltaic and wind turbine generator (SPV, WTG) as shown in Figure.1. Load models may use static and dynamic components to create consumption patterns that match real-world usage behavior. The entire nonlinear model undergoes linearization at an operating point which generates a state-space model that supports advanced control methods including PID and robust control and RL-based system design.

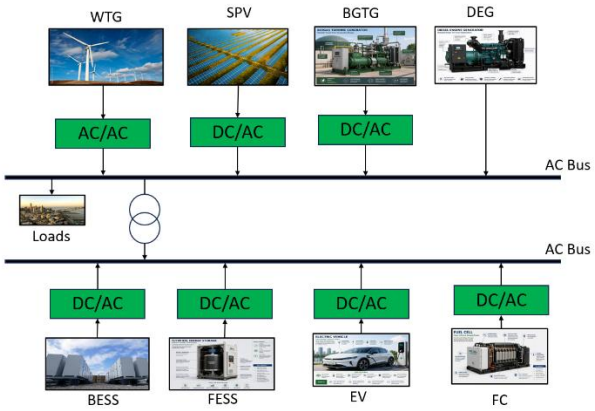


Figure1. General schematic of the IMGs including DG units and energy resources

2 .1 Diesel Engine Generator (DEG)

A diesel engine generator (DEG) is a commonly used electromechanical unit of energy conversion, which converts the chemical energy of diesel fuel into electrical power by using a coupled internal combustion engine and synchronous generator r [14]. A model of the first-order transfer functions is used to approximate the dynamic behaviour of a diesel engine generator (DEG) as in (1) [5].

$$TF_{DEG}(s) = \left(\frac{K_{DEG}}{1 + sT_{DEG}}\right)\left(\frac{K_T}{1 + sT_T}\right) \quad (1)$$

In equation (1) the parameters K_{DEG} and T_{DEG} are proportional to the system gain and the time constant of the distributed energy generator (DEG), respectively.

As shown in Figure 2, the analytical model of the DEG uses two important dynamic parameters, T_G and T_T respectively, which correspond to the time constants of the governor and turbine subsystems, respectively [15]. The complete transfer function of the DEG is established through the combination of governor dynamics and turbine dynamics which operate in a sequential

system. The system uses nonlinear elements which include saturation and sign functions to create physical constraint boundaries that define generator system operation limits.

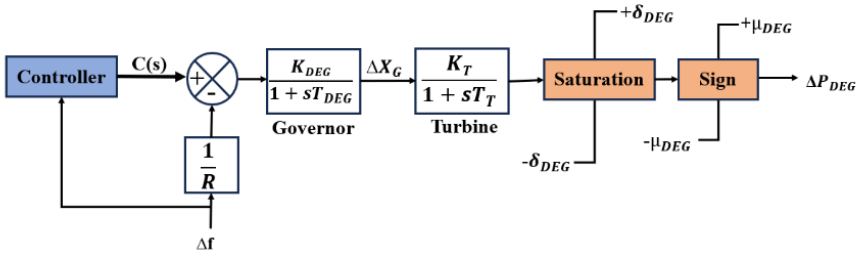


Figure 2. Mathematical representation of the diesel engine generator (DEG)

2 .2 Solar Photovoltaic (SPV)

SPV systems are a type of renewable energy technologies that directly transform solar irradiance into electrical energy by the photovoltaic effect [16].

A first-order transfer function can be used to effectively approximate the transient response of the SPV system. As shown in (2)

$$TF_{spv}(s) = \frac{K_{spv}}{1 + sT_{spv}} \tag{2}$$

The parameters K_{spv} and T_{spv} correspond to the system gain and time constant of the SPV unit, respectively. The analytical representation of a practical photovoltaic system model is shown in Figure 3.

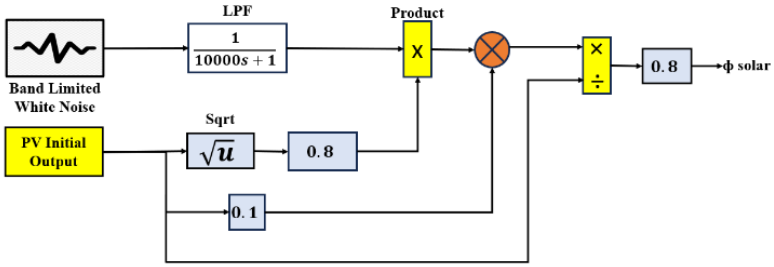


Figure 3. Analytical representation of SPV system

2 .3 Wind Turbine Generator (WTG)

is a renewable energy conversion system utilizing the kinetic energy of wind and converting it into electrical energy via a multi-stage electromechanical process [17].

The dynamic response of the WTG is sufficiently modeled by a first-order transfer function, as provided in (3)

$$TF_{WT}(s) = \frac{K_{WT}}{1 + sT_{WT}} \tag{3}$$

The WTG model uses parameters K_{WT} and T_{WT} to define system performance through system gain measurement and time constant evaluation. The WTG dynamic system is depicted through its analytical representation which scientists present in Figure 4 [18].

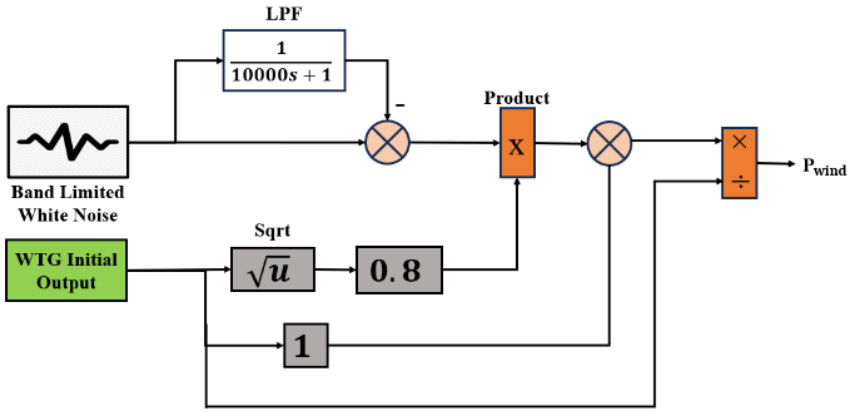


Figure 4. Analytical representation models for an operational WTG system

2 .4 Biogas Turbine Generator (BGTG)

is a dispatchable and renewable power generation system that transforms chemical energy of biogas into electrical energy in a thermodynamic and electromechanical conversion process[19].

The transfer function below can be analytically used to represent the dynamic properties of the Biogas Turbine Generator (BGTG):

$$TF_{BGTG}(s) = \frac{1 + sX_d}{(1 + sY_d)} \cdot \frac{1 + sT_{cri}}{1 + sT_{bgd}} \cdot \frac{1}{1 + sT_{btt}} \tag{4}$$

In (4), X_d, Y_d,d_v , T_{cri}, T_{bdg}, and T_{btt} These parameters, in that order, are the lead and lag time constants, the delay caused by actuator valve, the biogas transport delay, and the time constant of the discharge dynamics in the BGTG system.

2 .5 Fuel Cell (FC)

A Fuel Cell (FC) is an electrochemical cell that is capable of directly converting chemical energy of a fuel, usually hydrogen, into electrical energy without combustion by oxidation-reduction reactions [20]. a first-order lag model is used to represent the system and is approximated by the transfer function in Equation (5)

$$TF_{fc}(s) = \frac{K_{fc}}{1 + sT_{fc}} \tag{5}$$

K_{fc} and T_{fc} are the approximate values of the gain and time constant of the fuel cell model, respectively.

2 .6 Battery Energy Storage (BES)

Battery Energy Storage (BES) systems are electrochemical systems that store electrical energy as chemical energy and release them when needed by the power system. Uncontroversially, they are being utilized extensively in contemporary power networks (particularly in renewable-integrated and microgrid systems) because they can respond dynamically quickly and provide frequency regulation, as well as adding to the overall system reliability [21]. to describe and model the dynamic behavior of the system, a first-order transfer function as in Equation (6) is used.

$$TF_{BES}(s) = \frac{\Delta SOC(s)}{\Delta P_{BES}(s)} = \frac{K_{BES}}{1 + sT_{BES}} \tag{6}$$

K_{BES} and T_{BES} represent the approximated gain and time constant of the BESS model, respectively.

$$SOC_{Min} \leq SOC \leq SOC_{Max} \tag{7}$$

$\Delta SOC(s)$ is the difference between the actual and nominal operating state of charge. The $\Delta P_{BES}(s)$ term is equal to the power that is exchanged by the energy storage system with positive values being the charging mode and negative values being the discharging mode.

2 .7 Flywheel Energy Storage System (FESS) model

A Flywheel Energy Storage System (FESS) is a mechanically-electrically powered energy storage technology that stores energy as rotational kinetic energy in high-speed rotating mass (flywheel) [22]. The first-order transfer function is a common model of the system dynamics mathematically expressed as in Equation (8).

$$TF_{fess}(s) = \frac{K_{fess}}{1 + sT_{fess}} \tag{8}$$

K_{fess} and T_{fess} are parameters that are proportional to the estimated gain and time constant of the FESS model, respectively.

2 .8 Electric Vehicle (EV)

An Electric Vehicle (EV) is a transportation system that uses onboard energy storage devices to drive its electric traction motor which receives electrical energy from battery storage [23]. A first-order transfer function is used to model the dynamic behavior of the EV as shown in the analysis in Equation (9).

$$TF_{ev}(s) = \frac{K_{ev}}{1 + sT_{ev}} \tag{9}$$

where K_{ev} and T_{ev} are equal to the gain and the time constant of the EV model parameters respectively.

2 .9 Dynamics of the Generator Model

The generator model dynamics are a description of how a generator responds over time to changes in mechanical input power and electrical load demand in a power system [24]. The behavior of the generator can be modeled as a transfer function and this can be formulated in the following manner.

$$TF_{DG}(s) = \frac{1}{D + sM} \tag{10}$$

The dynamic control of the generator is based on the swing equation, which defines the characteristics of the generator's rotational motion [24]. In the equation (10), M is equal to the inertia constant, and D is equal to the damping coefficient.

$$\Delta P_{net} = P_s - P_l \tag{11}$$

The generated power is denoted by P_s and the required load power is denoted by P_l . This simplified model of a generator is believed to be very efficient in the modeling of the key dynamics needed to study LFC and to develop controllers in IMGs [25].

2 .10 Block Diagram of IMG

The block diagram of an Islanded Microgrid (IMG) of load frequency control (LFC) shows the general architecture of the system and the relationship between the key dynamic parts of the system in the autonomous operating conditions. It gives an effective accounting of how frequency variations are controlled by coordinated management of distributed generating units, energy storage systems (ESS) and load variations in the absence of a main grid connection. The Figure 5 is normally a representation of the feedback network to achieve system frequency and power balance within reasonable limits. A typical LFC-based IMG system is set up to provide local loads with multiple distributed energy resources (DERs) including renewable generation units, traditional dispatchable generators, and energy storage devices. The system frequency is continuously fed back to the control mechanism which produces corrective signals that are fed back to the system frequency. This feedback control system provides power balance between demand and generation. Dynamic performance is also improved by the presence of energy storage and fast responding units to offset disturbances in load and renewable intermittency. The equations (1, 2, 3, 4, 5, 6, 8 and 10) represent the mathematical models of the DGs and ESS. Table 1 indicates the first-order transfer functions and nominal values of each DG and

ESS in the model. In general, the block diagram is a basic instrument in the analysis of the stability of the system, the design of controllers and the performance of frequency regulation in islanded microgrid settings.

TABLE I. Equivalent first order transfer functions of DGUS and ESDS [26275]

DGUs/ESS	Equation Number	Parameters	Nominal Transfer Function
DEG	*1*	T_{DEG}= 0.08, K_{DEG}= 1 T_T= 0.4, K_T= 1	$\frac{K_{DEG}}{1+T_{DEG}s}$ $\frac{K_T}{1+T_Ts}$
SPV	*2*	T_{spv}= 0.8, K_{spv}= 1	$\frac{K_{spv}}{1+T_{spv}s}$
WTG	*3*	T_{WT}= 1.5, K_{WT}= 1	$\frac{K_{WT}}{1+T_{WT}s}$
BGTG	*4*	X_d= 0.6, Y_d= 1, d_v= 0.05, T_{cri}= 0.01, T_{bgd}= 0.23,	$\frac{1+sX_d}{(1+sY_d)(1+sd_v)}$ $\frac{1+sT_{cri}}{1+sT_{bgd}}$ $\frac{1}{1+sT_{btt}}$
FC	*5*	T_{fc}= 0.26, K_{fc}= 1	$\frac{K_{fc}}{1+T_{fc}s}$
BESS	*6*	T_{BES}= 0.1, K_{BES}= 1	$\frac{K_{BES}}{1+T_{BES}s}$
FESS	*8*	T_{fess}= 0.1, K_{fess}= 1	$\frac{K_{fess}}{1+T_{fess}s}$
EV	*9*	T_{ev}= 0.9, K_{ev}= 0.7	$\frac{K_{ev}}{1+T_{ev}s}$
DG	*10*	D=0.0015, M=0.1667	$\frac{1}{\mathrm{D}+\mathrm{sM}}$

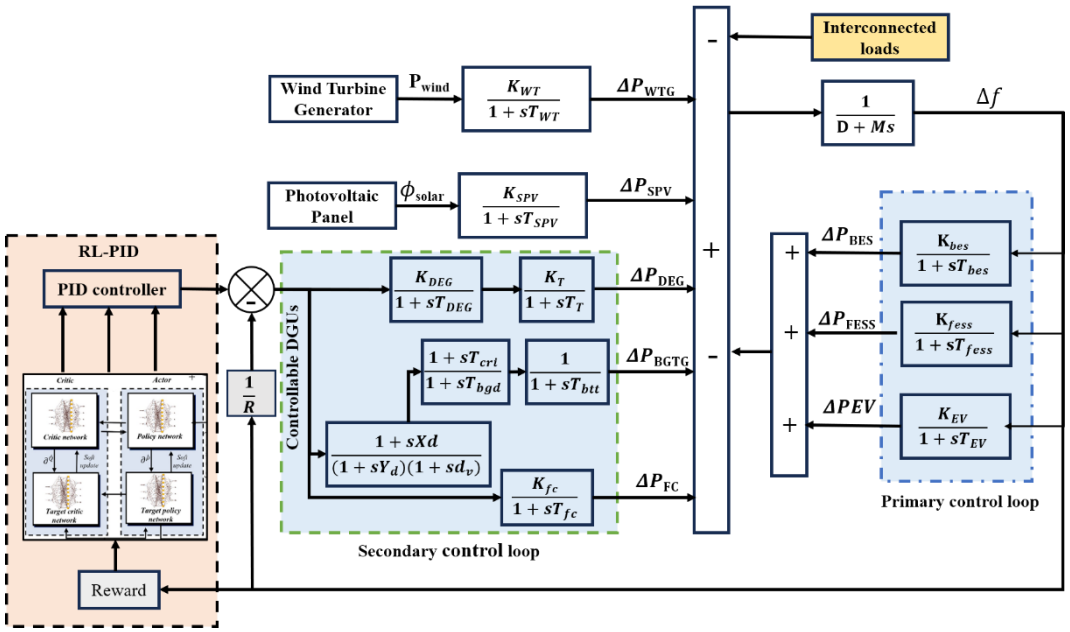


Figure 5. The diagram of the IMG system, which includes an RL agent adaptive PID regulator along with adjustable DGs and energy storage.

3 THE TWIN DELAYED DEEP DETERMINISTIC POLICY GRADIENT (TD3) ALGORITHM

represents a sophisticated actor-critic RL system which addresses two major challenges of value-based continuous control systems through its special design. The TD3 algorithm builds on the deterministic policy gradient foundation through its algorithmic enhancements which improve both convergence reliability and policy performance [28]. The method uses dual critic networks to decrease overestimation errors through its approach of selecting the lower valuation between two Q-value assessments which leads to better value estimation accuracy. The TD3 system uses time-differentiated policy changes to update its actor network at a slower rate than its critic networks because this method enables better value assessment prior to implementing system changes. The system uses target policy smoothing through its method of adding adjusted noise to the target action which helps the system function better under function approximation errors while stopping the policy from using areas with extreme value function peaks [29].

TD3 provides effective control for continuous control tasks through its capabilities to acquire stable control policies from real-world system interactions without needing formal system models. The off-policy learning design of the system increases its ability to learn from fewer samples which enables its use in challenging environments that include renewable power systems and island-based microgrid systems. The application of TD3 has increased in modern

control design systems because these systems require adaptive data-driven optimization methods to achieve better transient response and steady-state performance.

The TD3 algorithm structural framework is displayed in Figure 6 which shows that the control system operates through six separate neural networks. The system uses an actor network which creates control outputs together with its target actor and it also includes two critic networks with their respective target critics to achieve stable learning and policy assessment. [28].

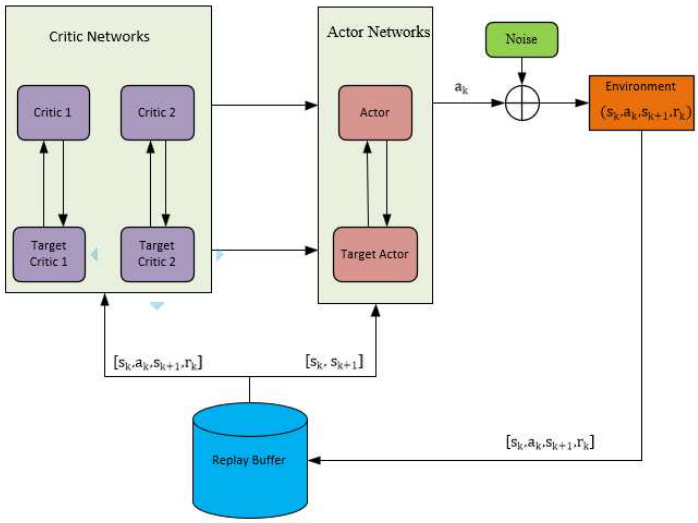


Figure 6. General structure of TD3 algorithm

In TD3, the parameters of the target networks are updated using a soft update system, which is a Polyak averaging update mechanism, in which a small coefficient τ controls the rate of update, and the approach is similar to that of DDPG. The entire description of the TD3 approach is provided in Algorithm 1[29].

ALGORITHM 1: SUMMARY OF THE PSEUDOCODE FOR THE TD3 ALGORITHM.
1: Set up the actor network π_θ and two critic networks Q_{w1} , Q_{w2} using random parameters w_1, w_2, and θ. **2:** Initialize weights of target networks: $\hat{w}_1 \leftarrow w_1$, $\hat{w}_2 \leftarrow w_2$, $\hat{\theta} \leftarrow \theta$ **3:** Initialize replay buffer B. Training Loop **for k= 1 to T do** **4:** Select action with exploration noise: $a_k \leftarrow \pi_\theta(s_k) + \eta, \qquad \eta \sim \text{noise}(0, \sigma)$ Execute a_k observe reward r_k and new state s_{k+1} **5:** Save transition $(s_k, a_k, s_{k+1}, r_k) \rightarrow B$ **6:** Sample mini-batch of N transitions

$$(s_i, a_i, r_i, s_{i+1}) \sim \mathrm{B}$$

Compute target action with policy smoothing:

$$a_k \leftarrow \hat{\pi}_{\theta'}(s_{i+1}) + \eta\,, \eta \leftarrow clip\,(N\,(0, \sigma), -c, c)$$

Compute target value

$$\varphi i \;\leftarrow r_i + \gamma . min\{\hat{Q}_{\hat{w}1}(\,\hat{a}_{i+1}, s_{i+1}), \hat{Q}_{\hat{w}2}(\,\hat{a}_{i+1}, s_{i+1})\}$$

7: Update the parameters for the critic:

$$w1 \leftarrow arg\,\min_{w1} \frac{1}{N} \sum \varphi i - Q_{w1}(s_i, a_i))^2$$

$$w2 \leftarrow arg\,\min_{w2} \frac{1}{N} \sum \varphi i - Q_{w2}(s_i, a_i))^2$$

8: delayed policy update (every d step):

Update actor using the deterministic policy gradient

$$\nabla_\theta J = \frac{1}{N} \sum_i (\nabla_a\, Q_{w1}(s_i, a_i) . \nabla_\theta \pi_\theta(s_i))$$

9: Update the target networks:

$$\hat{w}1 \leftarrow \tau \cdot w1 + (1\; -\; \tau) . \hat{w}1$$

$$\hat{w}2 \leftarrow \tau \cdot w2 + (1\; -\; \tau) . \hat{w}2$$

$$\hat{\theta} \leftarrow\; \tau . \theta + (1 - \tau) . \hat{\theta}$$

10: End for.

4 METHODS OF OPTIMIZATION OF PID CONTROLLER PARAMETERS.

The identification of optimum parameters for PID controllers has received a lot of interest because it directly influences the dynamic performance, margin of stability, and disturbance rejection ability [30].

Traditional tuning methods, like heuristics or rule-based tuning, can offer a reasonable starting point but fail to achieve optimal behaviour in the presence of nonlinearities and different operating conditions. Therefore, more current studies have turned to more formal optimization-based approaches, which cast PID tuning as a minimization of a predefined performance metric (i.e., ITAE, ISE, or settling time) [31]. This work has been done by a wide range of optimization techniques, such as intelligent optimization techniques like COA [15] and GWO-CS[11], which are the most popular metaheuristic algorithms because they can handle non-convex, multimodal search spaces without gradient information. Figure 7 presents a general outline of the steps in calculating the PID gains using a heuristic optimization algorithm. A heuristic-based optimization approach for determining the most suitable PID controller parameters generally entails a sequence of systematic steps designed to achieve enhanced control performance as follows:

Procedure for Selecting Optimal PID Gains Using Search Optimization Techniques
Step1: *Define the feasible search space for the decision variables:*

$$X = [K_p, K_i, K_d], X \in [X^{min}, X^{max}]$$

Step 2: *Define the objective function* $J(e)$ *, where the performance index is selected from:* $J(e)$ ∈**{ISE, IAE, ITAE, ITSE}**.

Step 3: *Select the optimization algorithm* L *from the candidate set:* L ∈**{GWO-CS, COA}**

Step 4: *Initialize the maximum number of iterations* T**,** *and population size* N**.**

Step 5: *For iteration* $k = 1$ to T

Step 6: *For each candidate solution* $r = 1$ **to** N

Step 7: *Generate or update candidate feasible solution* X_r

Step 8: *Evaluate the objective function for current population* r *and* $J_{(e)}^{k} \leftarrow X_r$

Step 9: *Update candidate solutions based on the optimization search rules and their corresponding objective values.*

End inner loop.

Step 10: *Calculate the objective function of all the feasible solutions in the current iteration* k

Step 11: *Store the best objective value of the current iteration:* $J_{Best}^{k} \leftarrow J(e)$

Step 12:

Step 12: *If* $k < T$ *increment iteration counter* $k = k + 1$ *and repeat; otherwise, end outer loop and return the optimal solution* X^* *and its corresponding objective value* $J(e)_{Best}^{T}$.

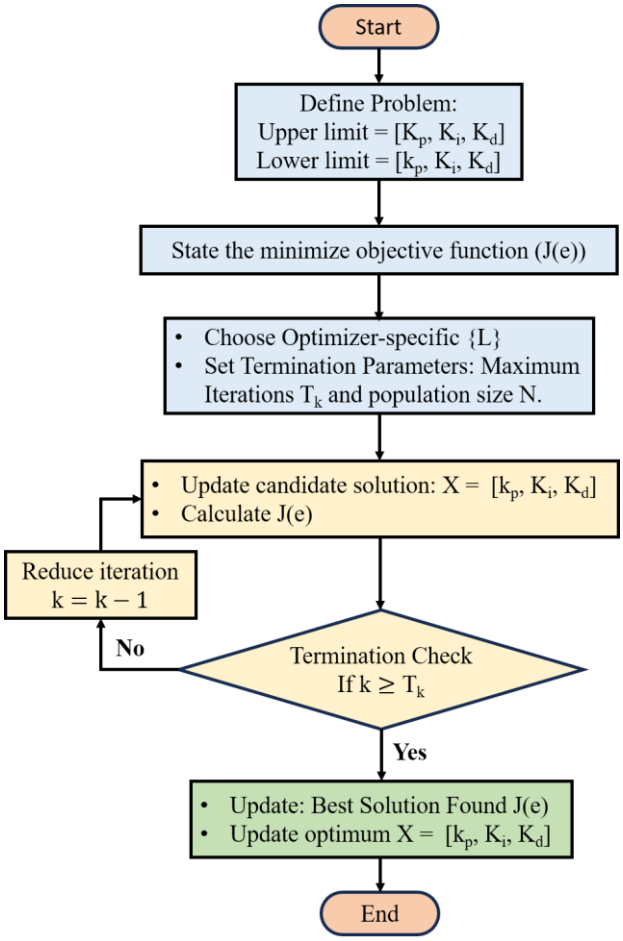


Figure 7. General flowchart explaining procedures for arriving at the best PID parameters using optimization methods

Recently, artificial intelligence techniques such as those based on RL have come into the limelight, which allow tuning of PID gains through interaction with the system environment with adaptivity and in real-time, thus improving robustness and real-time performance.

5 SIMULATION RESULTS

The proposed RL-based PID controller has been applied to control the IMG system and simulate its performance using MATLAB software. To demonstrate the effectiveness of the proposed method, the proposed TD3-PID controller has been compared with that of the COA-PID controller [15] and the CS-GWO-PID [11]. Two study cases were simulated to assess the proposed RL-based PID controller availability. These cases include (1) the IMG experiencing a step load change and (2) fluctuations that are damped with random steps.

All simulations are performed on a hardware configuration with a CPU Intel Core i7-13700H (2.40 GHz), 16 GB RAM, and the operation system Windows 11 64-bit. Furthermore, all simulations were conducted under the same computational conditions to ensure a fair comparison between the optimization algorithms.

5 .1 RL- Agent Based PID Tuning

This subsection presents the training process for the RL agent. The RL-based approach enables the controller to adaptively optimize the PID gains through interaction with the IMG environment. The training process for the RL agent involves multiple episodes, each consisting of a complete simulation of the power system that lasts 90 seconds. These simulations provide the necessary data for training the agent. The training settings for the RL agent are detailed in Table II. During each episode, the area's load demand varies from 0.025 to 0.075 p.u. to ensure that the agent is thoroughly trained to handle varying demand conditions.

Table II. RL -Agent Training Parameters.

Parameter	Value
Algorithms	TD3
Mini Batch Size (Samples per training update)	128
Total training episodes	1000
Experience Buffer Length	5 million
Sample Time (Ts)	0.25 s
Simulation Time	90 s
Max Steps per Episode	360
Score Averaging Window	10
Early Stopping (Stop based on threshold Episode)	30 Episode
Discount Factor	0.99
Target Smooth Factor	0.001

Learning rate for critic network	0.0001
Learning rate for actor network	0.00001
Optimizer	Adam
Standard deviation	0.01
Noise Decay Rate	0.00001

The episode reward is shown in Figure 8. Training is performed for 30 episodes with a simulation time of 90 s.

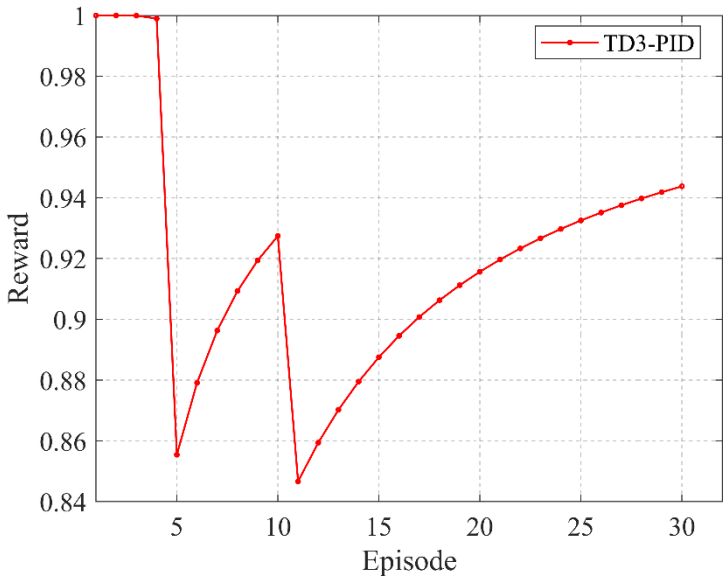


Figure 8. Episode reward during training process.

As illustrated in Figure 8, the reward progression highlights an initial phase of exploration, indicating improved control performance and successful policy convergence. The TD3 agent leverages past experiences stored in a replay buffer to incrementally learn an optimal policy, achieving a reward value of 0.86 before the final episode. The training period experiences sudden dips in the reward-episode figure, which can stem from two factors:

1) The agent explores unfamiliar state-action pairs by intentionally trying new actions to improve policy robustness, even though such actions may temporarily reduce performance.

2) Stochastic variations introducing unexpected dynamics that can challenge the controller and lead to short-term decreases in reward.

Furthermore, Figure 3 displays the evolution of the PID gains over the course of training. The gains converge to stable values after several episodes, reflecting the RL-agent ability to autonomously optimize PID parameters for reliable IMG performance. Figure 4 shows the validation nominal frequency and demand power tracking performance of the TD3-PID agent. The TD3-PID controller successfully achieved a frequency and power close to baseline values,

despite the inherent system noise and disturbances, demonstrating its capability for accurate closed-loop control.

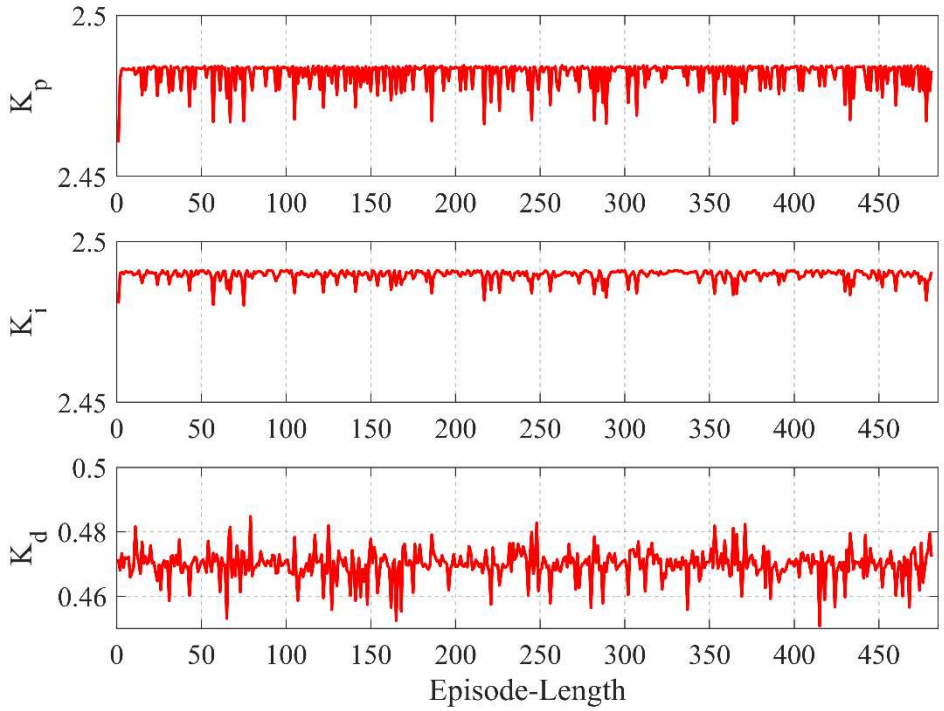


Figure 9. Evolution of PID gain parameters (Kp, Ki, Kd) over training episodes.

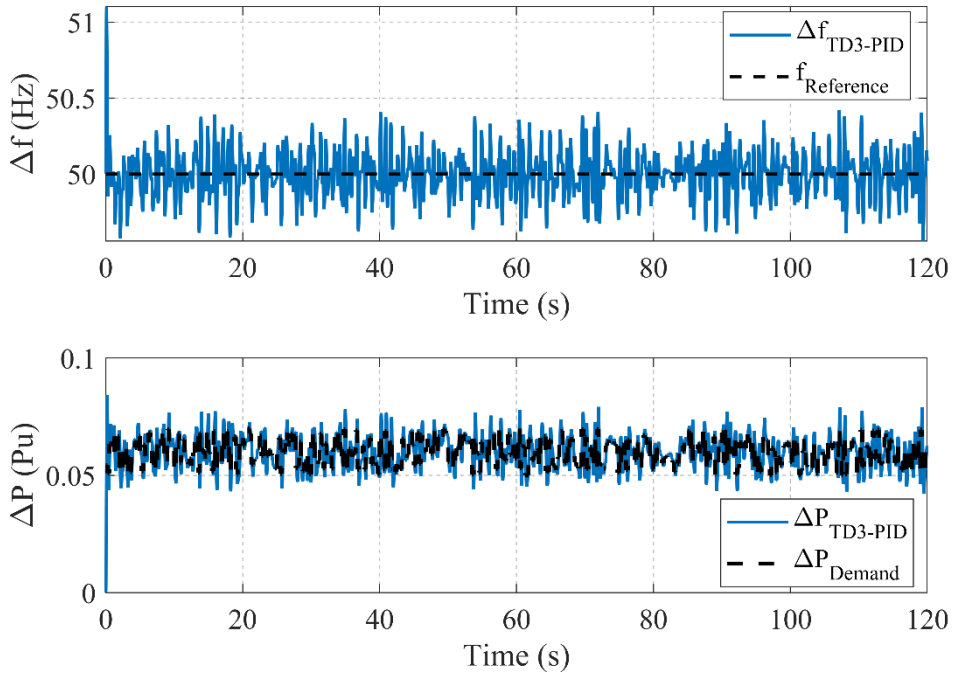


Figure 10. Validation performance of the closed-loop frequency and demand power tracking.

5.2 Optimization-Based PID Tuning

This research work incorporates two metaheuristic optimization algorithms, namely COA and CS-GWO. Both the COA and CS-GWO approaches were employed as evaluation approaches for the proposed TD3-Agent. Two optimization algorithms are employed to determine the optimal values of the PID controller gains by minimizing a predefined integral time-weighted absolute error (ITAE) as an objective function for the optimization problem. The initial configurations, which are common to two optimizers, are succinctly summarized in Table III.

Table III. Common Initialization Settings for the COA and CS-GWO Optimizers.

Settings	Value
Number of iterations	30
Population size	25
$[K_p, K_i, K_D]_{Lower}$	[0,0,0]
$[K_p, K_i, K_D]_{Upper}$	[10,10,10]

In addition, Table IV summarizes the PID gains obtained by each optimization algorithm during the tuning phase, subject to the predefined upper and lower bounds.

Table IV. Optimized PID Controller Gains for the IMG system.

Controller	K_p	K_i	K_D
CS-GWO-PID	5.46	10.00	1.16
COA-PID	7.51	9.59	1.22

The convergence curves of CS-GWO and COA optimization algorithms are shown in Figure 11, visually demonstrating their effectiveness in addressing the LFC challenges. As shown in the convergence curves, the performance analysis of the proposed PID controller, as optimized by the CS-GWO algorithm, demonstrates clear advantages over the COA-based algorithm.

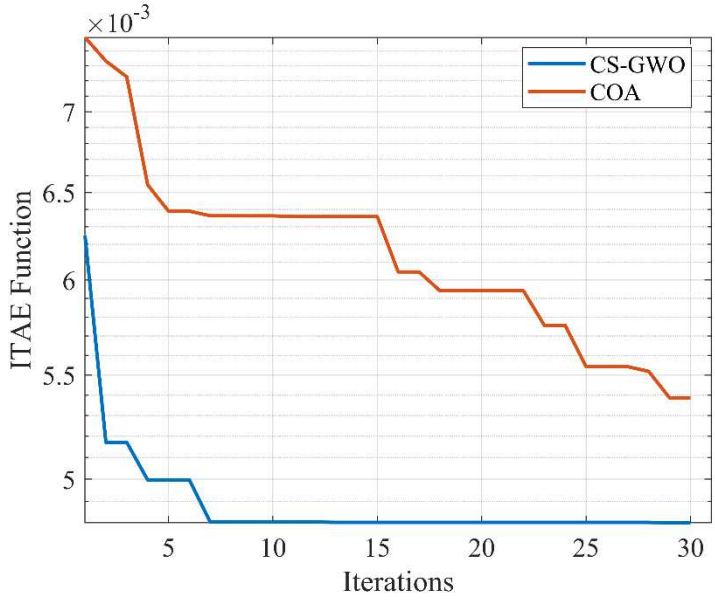


Figure 11. convergence curve.

A unit step change of 0.07 pu was applied to the IMG load to facilitate the design of controller parameters for the algorithm searching phase. The specific pattern of step load changes employed in the searching phase scenario is shown in Figure 12. In the time-domain responses, the CS-GWO-PID controller rapidly restores frequency deviations to the nominal value with minimal overshoot, while also ensuring smooth power adjustment.

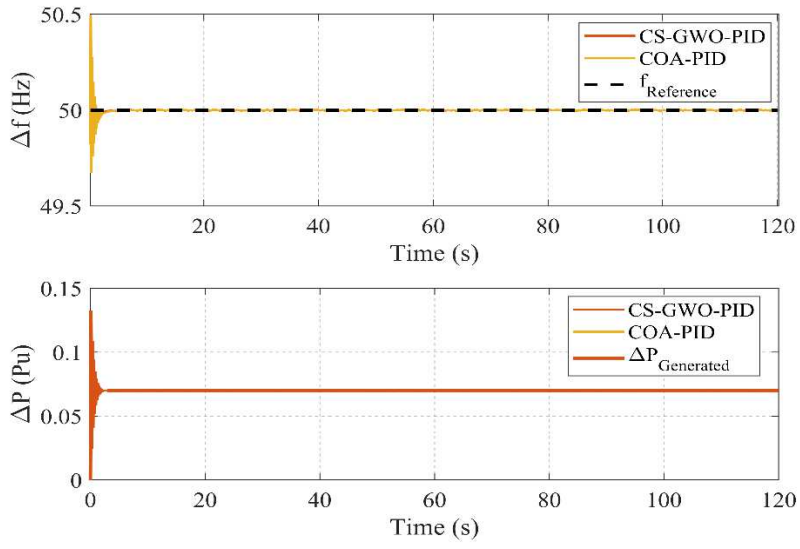


Figure 12. Frequency and Load-Pattern Responses of the CS-GWO-PID and COA-PID Controllers during Exploration and Exploitation Phases.

It is notable that the optimized controller parameters, which were obtained during the exploration and exploitation phases, were retained for use in the PID controller across all scenarios considered.

5 .2 Efficiency and Performance Evaluation

In this subsection, the proposed TD3-PID agent and considered tuning algorithms are evaluated in terms of controller performance metrics that include settling time, overshoots, undershoots, and numerical values of evaluation indices (ISE, ITSE, IAE, and ITAE). This analysis emphasizes the advantages of each approach based on simulation results and performance metrics. Figure 13 shows the variations in the output power of uncontrollable sources (WTG and PV systems) within the IMG under all studied scenarios.

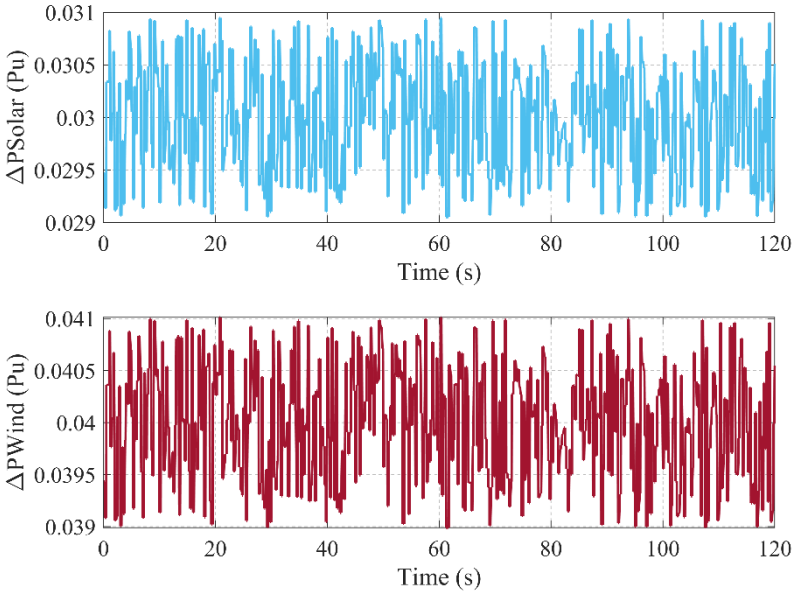


Figure 13. Output power of uncontrollable sources: wind turbine generators (WTG) and photovoltaic (PV) systems.

A) Studied Scenario 1: Power demand varies in a two-step pattern

A unit step change from 0.06 to 0.075 pu at half of the simulation period is applied to the IMG to define Scenario I. Figure 14 depicts the IMG frequency response with the specific pattern of step load changes employed. The TD3 agent and two optimization algorithms, CS-GWO-PID and COA-PID, achieve this result for the PID controller in Scenario I. The results highlight the superiority of the RL-based design, exhibiting faster response and improved performance indices compared to the other controllers. This observation demonstrates that the proposed

approach based on the TD3-agent PID is definitely a robust controller design in terms of IMG frequency regulation.

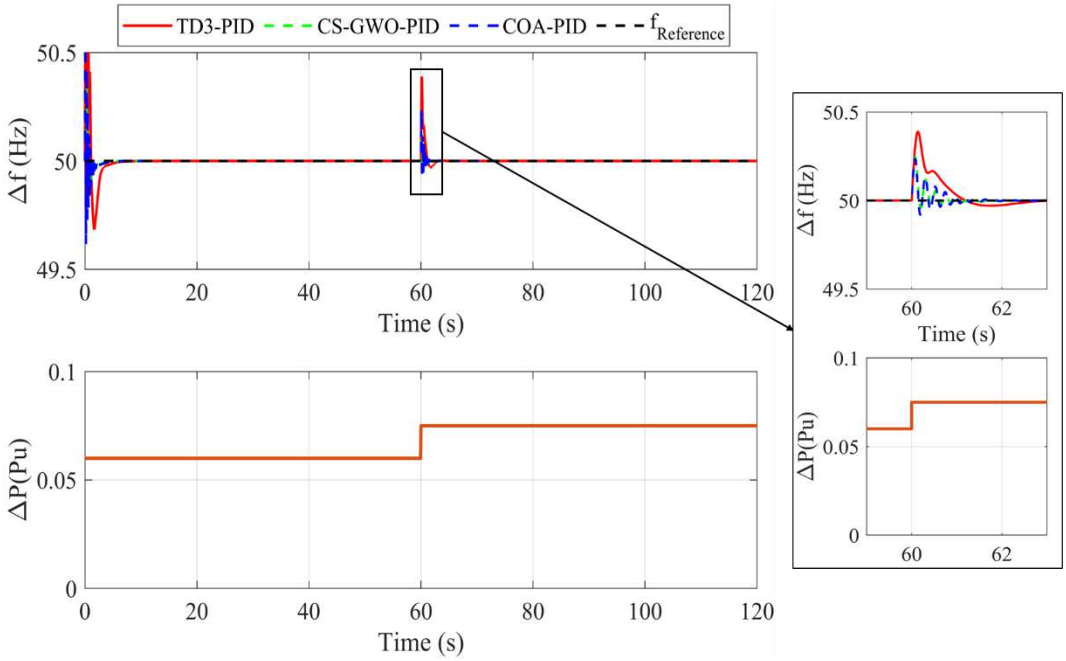


Figure 14. Frequency response of the IMG of different PID-based controllers under Scenario I.

Furthermore, Figure 15 illustrates controllable sources (DG, FC, and BGTG) whose outputs are dependent on deviations of Δf. Therefore, it shows the participation rates of each controllable source during load changes, with the DG unit exhibiting a higher involvement due to its faster dynamics.

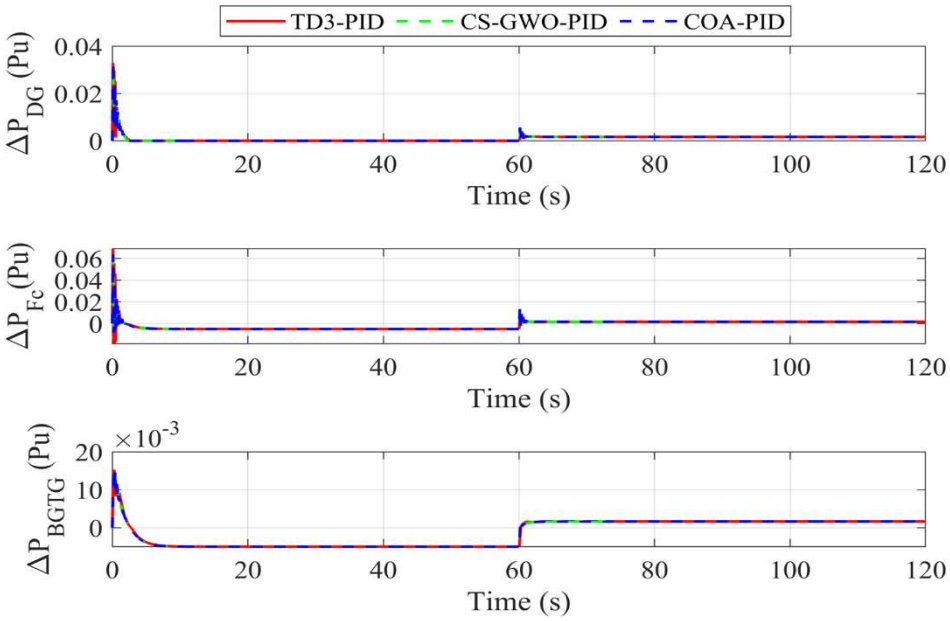


Figure 15. Changes in the output power of controllable sources (DG, FC, and BGTG) units within the IMG during scenario I.

In addition, the profiles of output power for the energy storage units, BESS, FESS, and EV units, operating in both charging and discharging modes, are shown in Figure 16. The ranges of power output of these storage units present the variable nature of charging/discharging ability among different types of energy sources in response to an increase or decrease in IMG frequency and therefore help keep the power balance and obtain frequency stability within a microgrid.

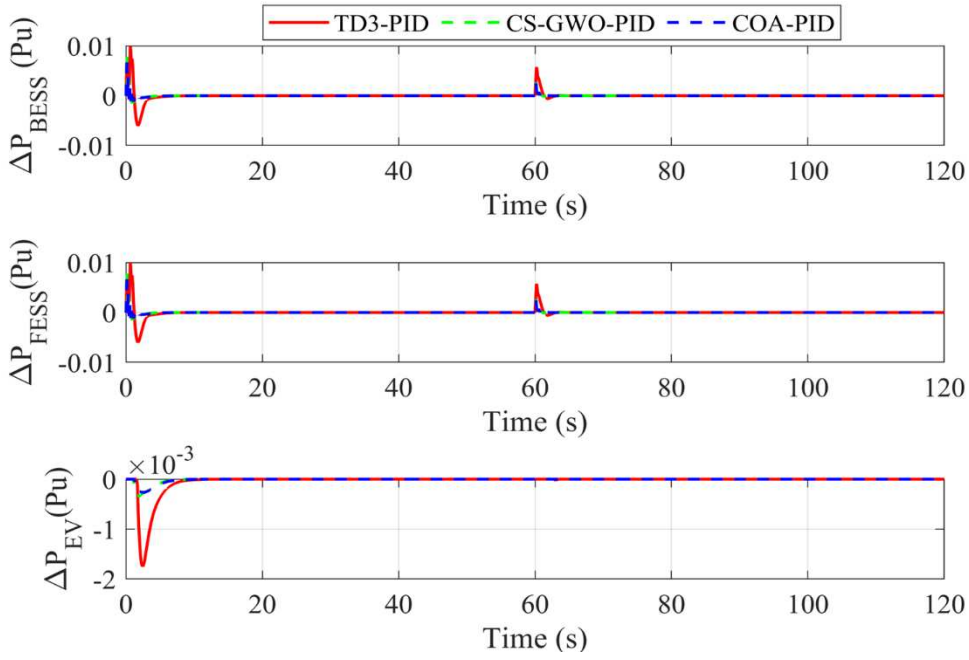


Figure 16. Variation in the Output Power of Storage Units under Scenario I.

Finally, the comparative evaluation of scenario I presents in Table V. a comprehensive comparison of the performance metrics of the investigated controllers, including settling time, overshoot, undershoot, and the corresponding evaluation indices, namely, ISE, IAE, ITAE, and ITSE. The obtained results clearly demonstrate the superiority of the proposed TD3-PID controller over the other control strategies. The proposed TD3-PID controller has a much faster settling time and better transient response characteristics. Moreover, its associated performance indices are found to be much lower compared with the alternative controllers, thus validating the proposed TD3-PID as an effective and robust solution.

Table V. Comparative Time-Domain Evaluation Results under Scenario I.

Metric	Proposed -TD3-PID	CS-GWO-PID	COA-PID
Undershoot	6.33E-01	5.44E-01	7.67E-01
Max Overshoot	1.45E+00	1.63E+00	1.57E+00
Settling Time	6.25E+01	6.11E+01	6.14E+01
ISE	1.05E-05	2.83E-05	3.15E-05
IAE	1.88E-02	5.89E-03	6.73E-03
ITAE	2.65E-02	7.09E-02	8.40E-02
ITSE	9.51E-05	1.51E-04	1.57E-04

B) Studied Scenario 2: Power demand varies in a stepwise pattern

To test the robustness of the proposed TD3-PID controller under realistic operating conditions, several time-varying load profiles were performed on the IMG during the simulation of realistic operating conditions. The load profiles are then randomly varied between a minimum of 0.02 pu and a maximum of 0.09 pu, respectively. The objective of this scenario is to investigate the controller's capability to maintain frequency regulation and ensure system stability under dynamic load variation. Figure 17 shows the frequency response under random step load disturbances for the TD3-PID, CS-GWO-PID, and COA-PID controllers. The results indicate that the proposed TD3-PID controller is more effective in suppressing frequency deviation and regulating load disturbances compared to the other controllers. In particular, the TD3-PID achieves faster damping characteristics and improved dynamic response compared with the CS-GWO-PID and COA-PID controllers.

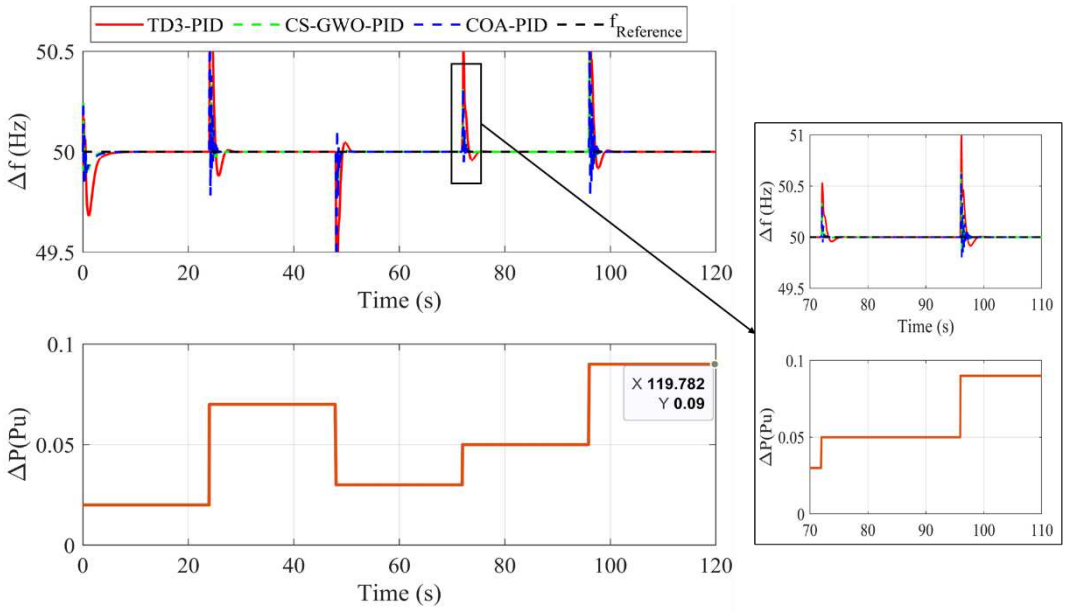


Figure 17. Frequency response for a TD3-PID controller, CS-GWO-PID controller, and COA-PID controller under scenario II.

Table VI confirms these observations by providing a comprehensive comparison of key time-domain indices for the CS-GWO-PID and COA-PID controllers based on the optimization algorithms and proposed TD3-PID. These indices include settling time, overshoot, undershoot, and the numerical values of evaluation indices (ITAE, ITSE). This comparison facilitates the identification of the most effective considered controller approaches.

Figures 18 and 19 illustrate the output power variations of various sources within the IMG during scenario II. The power contribution from each controllable source (DG, FC, and BGTG) and each storage unit (FESS, BESS, EV) approximately mirrors the observations from Scenario II.

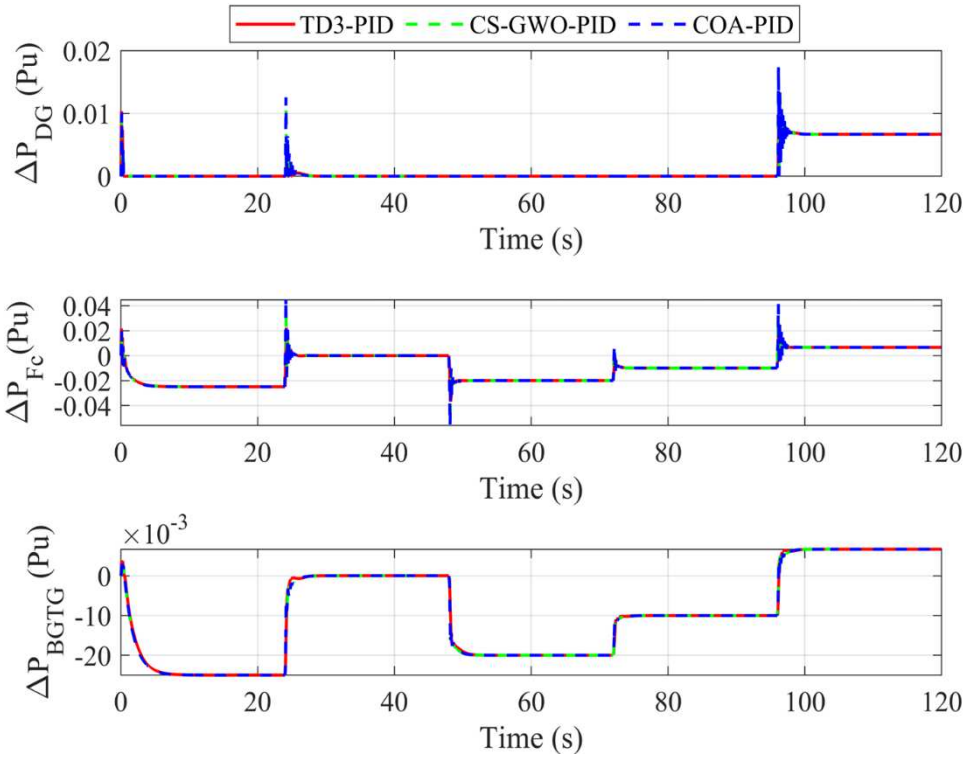


Figure 18. Changes in the output power of controllable sources (DG, FC, and BGTG) units within the IMG during scenario II.

The power fluctuations of the storage devices, including the FESS, EV, and BESS units, reflect their charging and discharging behaviours in response to load demand variations and power balance constraints within the system.

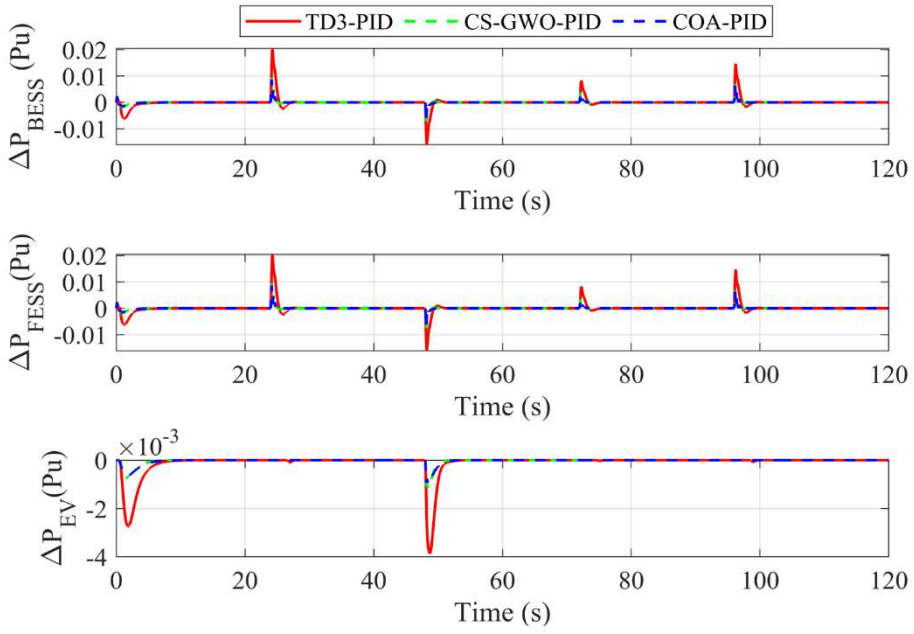


Figure 19. Variation in the Output Power of Storage Units under Scenario II.

Table VI. Comparative Time-Domain Evaluation Results under Scenario II.

Metric	Proposed -TD3-PID	CS-GWO-PID	COA-PID
Undershoot	2.07E+00	1.30E+00	1.25E+00
Max Overshoot	2.63E+00	1.64E+00	1.58E+00
Settling Time	9.88E+01	9.76E+01	9.79E+01
ISE	4.79E-05	7.16E-05	6.83E-05
IAE	5.21E-02	1.37E-02	1.44E-02
ITAE	2.28E+00	5.77E-01	6.29E-01
ITSE	2.16E-02	3.39E-03	3.32E-03

5 .3 Observations on the demand-change scenarios

The proposed TD3-PID controller integrates TD3 algorithms with PID to improve the robustness and adaptability of LFC in the dynamic IMG system. The time-domain response curves and the quantitative performance indicated in Tables V, VI, and VII confirm a strong potential of the proposed TD3-PID to handle sudden load changes and stochastic disturbances across various load demand conditions.

In Scenario I, which involves a single-step load disturbance, the TD3-PID controller achieves a noticeable reduction in all integral performance metrics (ISE, IAE, ITAE, and ITSE). All of the above improvements equate to the fact that the TD3-PID is a controller designed such that over time, there will be minimal deviation of cumulative frequency change: a key requirement for stable system operation. TD3-PID can provide a slightly smoother response with slightly greater maximum overshoot than CS-GWO-PID and COA-PID but still has a competitive settling time and moderate undershoot. This balance allows the controller to react quickly to disturbances but also contain overall system deviation within tolerable limits.

Scenario II presents multiple sequential disturbances that test the controller's adaptability and robustness, featuring many consecutively repeated disturbances. In this scenario, TD3-PID consistently provides excellent frequency regulation with a settling time that is very close to those of the reference controllers. The metrics based on the error, namely the integral of squared error and the integral of absolute error, remain positive, showing that TD3-PID is effective at suppressing oscillations and returning quickly to quasi-steady-state conditions. However, the data also reveal that both undershoot and overshoot values increase under more complex disturbance profiles. This trend can be attributed to the nature of TD3, which teaches aggressively and prioritizes quick compensation over minor excursions. Nevertheless, low steady-state error values are an indication that a controller has the potential to maximize long-term performance.

5 .4 Impact of System Parameter Variations

This subsection investigates the robustness of the TD3-PID controller under parametric uncertainties caused by modeling variations. Specifically, the effects of varying the following parameters by ±25% from their nominal values are analyzed: inertia constant (M), load damping coefficient (D), fuel cell time constant T_{FC}, and governor time constant T_{DEG}. The IMG performance is evaluated under a 0.07 pu step load disturbance. In the uniaxial sensitivity analysis, only one parameter is varied at a time while all other parameters are maintained at their nominal values. To further evaluate the robustness of the IMG against broader parameter uncertainties, a multiaxial sensitivity analysis is also performed. In this case, all defined parameter variations are simultaneously applied to the IUMG model.

Figure 20 illustrates the IMG frequency response of the TD3-PID controller under both uniaxial and multiaxial sensitivity analyses. The corresponding time-domain evaluation indices are presented in Table VIII. As observed in Table VIII, the influence of uncertainty for each parameter on IMG performance under single-execution conditions shows that the deviations of obtained time-domain indices from nominal values remain relatively small, which highlights the robustness and stability of the proposed TD3-PID controller in relation to the uncertainties in the controller parameters.

Table. VIII. Comparison of Time-Domain Evaluation Indices in Uniaxial and Multiaxial Sensitivity Analyses.

Parameter	Range changes (%)	Settling time (s)	Undershoot (%)	Overshoot (%)	ITAE	ITSE×10^{-13}
M	-25%(Uniaxial)	0.0429	0.323	3.592	0.022	9.60
	-25%(Multiaxial)	0.0432	3.153	3.222	0.031	9.60
	Normal	0.0428	0.230	3.093	0.022	5.40
	+25%(Multiaxial)	0.0428	0.234	2.763	0.022	3.45
	+25%(Uniaxial)	0.0428	0.234	2.763	0.022	3.45
D	-25%(Uniaxial)	0.0428	0.230	3.093	0.022	5.40
	-25%(Multiaxial)	0.0432	3.153	3.222	0.031	9.60
	Normal	0.0428	0.230	3.093	0.022	5.40
	+25%(Multiaxial)	0.0428	0.230	3.093	0.022	5.40
	+25%(Uniaxial)	0.0428	0.230	3.093	0.022	5.40
T_{FC}	-25%(Uniaxial)	0.0430	0.228	2.848	0.021	5.40
	-25%(Multiaxial)	0.0432	3.153	3.222	0.031	9.60
	Normal	0.0428	0.230	3.093	0.022	5.40
	+25%(Multiaxial)	0.0427	0.330	3.283	0.023	5.40
	+25%(Uniaxial)	0.0427	0.330	3.283	0.023	5.40
T_{DEG}	-25%(Uniaxial)	0.0429	0.230	3.000	0.021	5.40
	-25%(Multiaxial)	0.0432	3.153	3.222	0.031	9.60
	Normal	0.0428	0.230	3.093	0.022	5.40
	+25%(Multiaxial)	0.0428	0.229	3.162	0.022	5.40
	+25%(Uniaxial)	0.0428	0.229	3.162	0.022	5.40

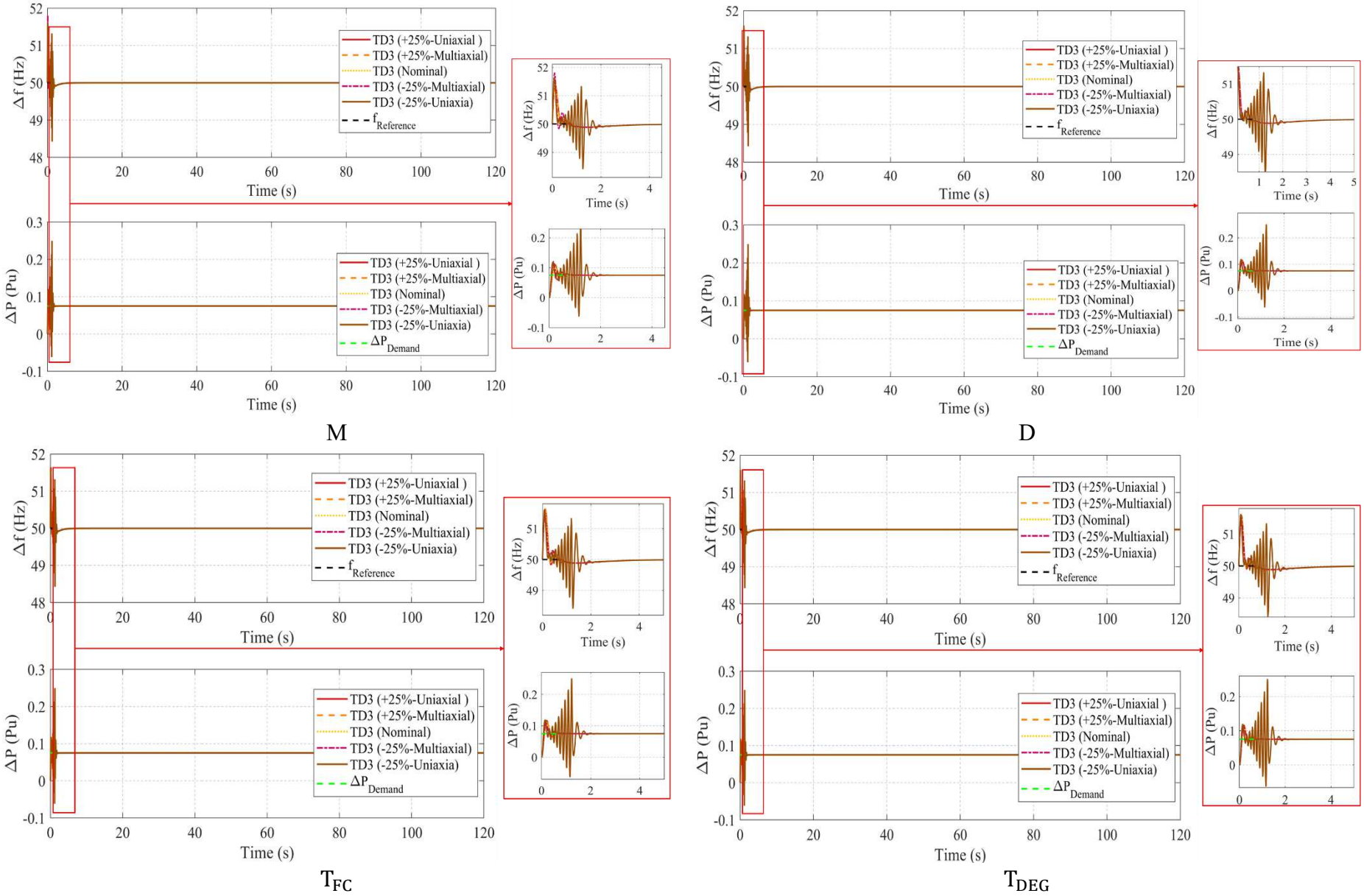


Figure 20. Uniaxial and multiaxial comparisons of IMG frequency responses for the TD3-PID controller.

The results of the sensitivity analysis presented in Table VIII and Figure 20 give substantial insight into the robustness of the TD3-PID controller in the presence of parametric uncertainties. For all cases the settling time was practically the same at 0.043 sec, proving the controller's fast dynamic response for any parameter shifts. In particular, moderate variations in undershoot and overshoot values were obtained when considering uniaxial changes; however, both ITAE and ITSE performances remained low and stable. In multiaxial scenarios, the system showed larger deviations with an atypical reliance on undershoot (upper half–third) quantification, which grew significantly negative alongside parameter shifts. Despite these deviations, the controller was able to maintain acceptable transient and steady-state performance in all tested scenarios. The curves of frequency response results in Figure 20 further reinforce these results.

In addition, the TD3-PID controller tracked the reference signal and rejected disturbances, whereas others were not so robust to parameter variations. The most significant degradation happened for all parameters in the case of negative multiaxial. However, in general terms, the metrics indicate that frequency and power deviations remain within practical limits.

6 CONCLUSION

This paper presented a novel approach for LFC in an IMG by integrating a RL-agent with an optimized PID controller. The performance of the proposed TD3-PID controller was evaluated under various operating scenarios within the IMG system. Comparative analyses were conducted against optimized PID controllers designed using the CS-GWO and COA algorithms. Simulation results demonstrated improved frequency response characteristics, indicating the effectiveness of the proposed control strategy under the investigated operating condition. Furthermore, robustness analysis was performed by applying ±25% variations to key system parameters, confirming the resilience of the TD3-PID controller against parameter uncertainties.

The parametric analysis suggested that the proposed TD3-PID controller is adaptable and effective under the investigated operating conditions. The proposed RL-TD3 PID controller demonstrated improved performance over the compared methods under the investigated islanded microgrids scenarios. In addition, the integral error indices remained relatively low under both uniaxial and multiaxial uncertainty conditions, demonstrating strong robustness against time-varying system parameters.

Although certain scenarios exhibited relatively higher transient responses, the TD3-PID controller consistently maintained stable operation and accurate reference tracking. By combining the real-time adaptability of deep RL with the simplicity and reliability of classical PID control, the proposed approach achieved fast transient performance together with effective long-term frequency regulation.

6 .1 Limitations and Future Work

The results presented in this paper are based on simulation studies of a renewable-based IMG for the operating scenarios and uncertainty conditions considered. The proposed TD3-PID controller exhibited promising performance compared to selected benchmark optimization algorithms, but its effectiveness has not been validated by hardware in the real-time experimental implementation. However, the selected optimization algorithm delivered slightly exceeded the proposed RL-TD3-PID in some tested disturbance scenarios.

In addition, the controller was also tested for the system configuration and disturbance scenarios considered in this work. Thus, the performance of TD3-PID under different microgrid topologies, communication delays, renewable disturbance scenarios, and larger-scale interconnected power systems needs to be investigated further. Future work will be dedicated to experimental validation and to the extension of the proposed control framework to more complex and practical microgrid environments.

Funding: This research was funded by the Deanship of Scientific Research at Northern Border University, Arar, KSA, for funding this research (through the project number NBU-FFR-2026-2124-04).

Data Availability Statement: The program files associated with this work will be available upon request or by corresponding with the authors.

Competing interests: Authors declare no competing interests.

Acknowledgments: The authors acknowledge the Deanship of Scientific Research at Northern Border University, Arar, KSA, for funding this research (project number NBU-FFR-2026-2124-04).

Author Contributions

- **Dana Rajaa Shaaban:** Conceptualization, methodology, investigation, formal analysis, writing – original draft, visualization.
- **Ali Nasser Hussain:** Conceptualization, methodology, supervision, writing—review & editing, correspondence.
- **Ahmed K. Ali:** Writing, review and editing, formal analysis, data curation, software, and validation.
- **Mohammed Alruwaili**: Resources, funding acquisition, formal analysis, writing– review & editing.
- **Moustafa Ahmed Ibrahim***: Responsible for supervision, project administration, methodology, validation, writing– review & editing, and correspondence.

References:

1. Yusuf, S. S., Kunya, A. B., Abubakar, A. S. & Salisu, S. Review of load frequency control in modern power systems: a state-of-the-art review and future trends. *Electr. Eng.* **107**, 5823–5848 (2025).
2. Su, T., Zhao, J., Yao, Y., Selim, A. & Ding, F. Safe reinforcement learning-based transient stability control for islanded microgrids with topology reconfiguration. *IEEE Trans. Smart Grid* (2025).
3. Shaaban, D. R. *et al.* Adaptive PID-based deep reinforcement learning for load frequency control in islanded microgrids with heterogeneous resources and energy storage. *Sci. Rep.* 0–47 (2026). doi:10.1038/s41598-026-50830-6
4. Hazem, Z. Ben, Saidi, F., Guler, N. & Altaif, A. H. A hybrid reinforcement learning framework combining TD3 and PID control for robust trajectory tracking of a 5-DOF robotic arm. *Automation* **6**, 56 (2025).
5. Bashishtha, T. K., Singh, V. P., Yadav, U. K. & Varshney, T. Reaction curve-assisted rule-based pid control design for islanded microgrid. *Energies* **17**, 1110 (2024).
6. Akter, A. *et al.* A review on microgrid optimization with meta-heuristic techniques: Scopes, trends and recommendation. *Energy Strateg. Rev.* **51**, 101298 (2024).
7. Rajalwal, N. K. & Acharya, D. S. Evolutionary Algorithms for Load Frequency Control of

Renewable Microgrid. in *Smart Grid 3.0: Computational and Communication Technologies* 153–184 (Springer, 2023).

8. Madhusudanan, G. & Padhmanabhaiyappan, S. Enhancing photovoltaic system flexibility: a novel integrated converter with COA optimization approach. *Renew. Energy Focus* **57**, 100808 (2026).
9. Ray, P. K., Bartwal, A. & Puhan, P. S. Load frequency control in interconnected microgrids using Hybrid PSO–GWO based PI–PD controller. *Int. J. Syst. Assur. Eng. Manag.* **15**, 4124–4142 (2024).
10. Singh, Kshetrimayum Millaner and Gope, S. Renewable energy integrated multi-microgrid load frequency control using grey wolf optimization algorithm. *Mater. Today Proc.* (2021). doi:10.1016/j.matpr.2021.02.035
11. Bouaddi, A., Rabeh, R. & Ferfra, M. Results in Engineering Load frequency control in autonomous microgrids using hybrid Algorithm GWO-CS based fuzzy logic sliding mode controller. *Results Eng.* **25**, 104412 (2025).
12. Dashtdar, M. *et al.* Frequency control of the islanded microgrid based on optimised model predictive control by PSO. *IET Renew. Power Gener.* **16**, 2088–2100 (2022).
13. Ahmadi, H., Shafiee, Q. & Bevrani, H. Mathematical modeling of islanded microgrid with static and dynamic loads. *Nexo Rev. Científica* **34**, 886–905 (2021).
14. Firah, A., Birane, M. & Degla, A. Techno-economic based optimization of photovoltaic/battery/diesel generator microgrid. *Rev. Roum. des Sci. Tech. Série Électrotechnique Énergétique is a J.* **70**, 447–452 (2025).
15. Davoudkhani, Iraj Faraji and Zare, Peyman and Abdelaziz, Almoataz Y and Bajaj, Mohit and Tuka, M. B. Robust load-frequency control of islanded urban microgrid using 1PD-3DOF-PID controller including mobile EV energy storage. *Sci. Rep.* **14**, 13962 (2024).
16. Li, C. *et al.* Assessing solar-to-PV power conversion models: Physical, ML, and hybrid approaches across diverse scales. *Energy* **323**, 135744 (2025).
17. Ahmed, S. D., Al-Ismail, F. S. M., Shafiullah, M., Al-Sulaiman, F. A. & El-Amin, I. M. Grid integration challenges of wind energy: A review. *Ieee Access* **8**, 10857–10878 (2020).
18. Zenhom, I. A., Marei, M. I. & Mohamed, A. M. I. Modelling, analysis, and stability

assessment of wind turbine generator connected to a low inertia AC-DC microgrid with frequency support capability. *Sci. Rep.* (2025).

19. Gholizadeh, T., Ghiasirad, H., Rostami, S. & Skorek-Osikowska, A. A biogas-fired cogeneration (cooling and power) system combined with biomethane facilities: 3E evaluation, sensitivity analyses and optimization. *Environ. Dev. Sustain.* **28**, 3791–3843 (2026).
20. Fang, T., von Jouanne, A. & Yokochi, A. Review of Electrochemical Systems for Grid Scale Power Generation and Conversion: Low-and High-Temperature Fuel Cells and Electrolysis Processes. *Energies* **18**, 2493 (2025).
21. Yin, K., Xiao, Y., Shen, X., Zhu, Y. & Yang, Y. Review of photovoltaic–battery energy storage systems for grid-forming operation. *Batteries* **10**, 288 (2024).
22. Xu, K., Guo, Y., Lei, G. & Zhu, J. A review of flywheel energy storage system technologies. *Energies* **16**, 6462 (2023).
23. Zhao, C. *et al.* Electric Vehicle Behavior Modeling for Vehicle-to-Grid Integration: Methods, Challenges, and Perspectives. *Energies* **19**, 871 (2026).
24. Murad, N., Kamarudin, M. N., Hanafi, A. N., Rozali, S. M. & Ibrahim, M. A. Exploration of characteristic equation towards the analysis of dynamical stability for synchronous generators through swing equation. *Int. J. Electr. Eng. Appl. Sci.* **7**, (2024).
25. Wu, M., Ma, D., Xiong, K. & Yuan, L. Optimizing load frequency control in isolated island city microgrids: A deep graph reinforcement learning approach with data enhancement across extensive scenarios. *Front. Energy Res.* **12**, 1384995 (2025).
26. Nabizadeh, F. & Bakhshinejad, A. Intelligent frequency control in AC microgrids using fuzzy logic. *Majlesi J. Mechatron. Syst.* **11**, 7–16 (2022).
27. Barik, A. K. & Das, D. C. Expeditious frequency control of solar photovoltaic/biogas/biodiesel generator based isolated renewable microgrid using grasshopper optimisation algorithm. *IET Renew. Power Gener.* **12**, 1659–1667 (2018).
28. Muktiadji, R. F., Ramli, M. A. M. & Milyani, A. H. Twin-Delayed Deep Deterministic Policy Gradient Algorithm to Control a Boost Converter in a DC Microgrid. *Electron.* **13**, 433 (2024).
29. Nasti, S. M., Najar, Z. A. & Chishti, M. A. Adaptive mapless mobile robot navigation

using deep reinforcement learning based improved TD3 algorithm. *Front. Robot. AI* **12**, 1625968 (2025).

30. Pavon, W. Metaheuristic-Based PID Controller Design with MOOD Decision Support Applied to Benchmark Industrial Systems. *Electronics* **14**, 3630 (2025).

31. Abbas, I. A. & Mustafa, M. K. A review of adaptive tuning of PID-controller: Optimization techniques and applications. *Int. J. nonlinear Anal. Appl.* **15**, 29–37 (2024).